Icarus 210 (2010) 713–721

Contents lists available at ScienceDirect

Icarus

journal homepage: www.elsevier.com/locate/icarus

Boulders and ponds on the Asteroid 433 Eros

Andrew J. Dombard [a,*], Olivier S. Barnouin [a], Louise M. Prockter [a], Peter C. Thomas [b]

[a] The Johns Hopkins University Applied Physics Laboratory, 11100 Johns Hopkins Rd., Laurel, MD 20723, United States
[b] Center for Radiophysics and Space Research, Cornell University, Ithaca, NY 14853, United States

ARTICLE INFO

Article history:
Received 28 January 2009
Revised 2 July 2010
Accepted 3 July 2010
Available online 14 July 2010

Keywords:
Asteroids, Surfaces
Asteroid Eros
Geological processes

ABSTRACT

There are ~300 features on the Asteroid 433 Eros that morphologically resemble ponds (flat-floored and sharply embaying the bounding depression in which they sit). Because boulders on Eros are apparently eroding in place and because ponds with associated boulders tend to be larger than ponds without blocks, we propose that ponds form from thermally disaggregated and seismically flattened boulder material, under the assumption that repeated day/night cycling causes material fatigue that leads to erosion of the boulders. Results from a simple boulder emplacement/thermal erosion model with boulders emplaced in a few discrete events (i.e., large impacts) match well the observed size distribution. Under this scenario, the subtle color differences of ponds (somewhat bluer than the rest of the surface) might be due to some combination of less space-weathered material and density stratification of silicate-rich chondrules and more metal-rich matrix from a disaggregated boulder. Volume estimates of ponds derived from NEAR Laser Rangefinder profiles are consistent with what can be supplied by boulders. Ponds are also observed to be concentrated in regions of low slope and high elevation, which suggests the presence of a less mobile regolith and thus a contrast in the resistance to seismic shaking between the pond material and the material that makes up the bounding depression. Future tests include shake-table experiments and temperature cycling (fatigue) of ordinary chondrites to test the thermal erosion mechanism.

1. Introduction

"Ponds" are features on the Asteroid 433 Eros that are thus far observed to be unique in the Solar System (Robinson et al., 2001; Veverka et al., 2001b). Morphologically, they are flat-floored (Cheng et al., 2002a) and often sharply embay the bounding depression in which they sit (Fig. 1), thus the description as ponds. Ponds appear to be smooth, indicating that the material is finer-grained (i.e., sub-cm) than the best resolution of the NEAR-Shoemaker images (Robinson et al., 2001). One of us (PCT) has constructed a database of 334 ponds (cf. Robinson et al., 2001). While ponded deposits can reach sizes of ~210 m across, the majority are <60 m wide. Most ponds are found on the bulbous ends of the elongated asteroid (Robinson et al., 2001, 2002; cf. Fig. 2).

Color images indicate only relatively subtle differences from the rest of the surface, with ponds possessing somewhat bluer colors (Robinson et al., 2001; Riner et al., 2006). These color characteristics have been attributed to (1) the presence of very fine-grained material (<50 μm), (2) a lack of space weathering of the pond material, or (3) a sorting process that separates silicate-rich pond material from the silicate-plus-metal composition of Eros (Robinson et al., 2001). Detailed analysis of NEAR-Shoemaker Multi-Spectral Imager color sequences indicates that none of these mechanisms alone can explain the color characteristics of ponds, although some combination may (Riner et al., 2006).

The spin axis of Eros is nearly in its orbital plane, giving the asteroid an obliquity of ~88°. Consequently, a band near the equator spends the most time at low Sun angles and hence experiences more terminator passages. This effect is an extreme example of the same effect on Earth where the high arctic regions spend most of the year either in full Sun or in darkness, and thus experience far fewer terminator passages than lower latitude regions. Based on an observed spatial correlation between the location of most ponds and areas of the surface that spend more time in near-terminator conditions (Fig. 3), electrostatic levitation of a very fine-grained component of the regolith of Eros has been proposed to be crucial in the formation of ponds (Robinson et al., 2001). Modeling has demonstrated the plausibility of electrostatic dust transport on Eros (Colwell et al., 2005; Haugsjaa and Colwell, 2006; Hughes et al., 2008) as a delivery mechanism of pond material to within a bounding depression, although seismic shaking (e.g., Cheng et al., 2002a) has been invoked to flatten this material to the observed pond morphology. Alternatively, Cheng et al. (2002a) proposed that the pond material derives from the flanks of the bounding depression seismically shaken down to the depression's

* Corresponding author. Present address: Department of Earth and Environmental Sciences (MC-186), University of Illinois at Chicago, 845 W. Taylor St., Chicago, IL 60607-7059, United States. Fax: +1 312 413 2279.
E-mail address: adombard@uic.edu (A.J. Dombard).

0019-1035/$ - see front matter © 2010 Elsevier Inc. All rights reserved.
doi:10.1016/j.icarus.2010.07.006

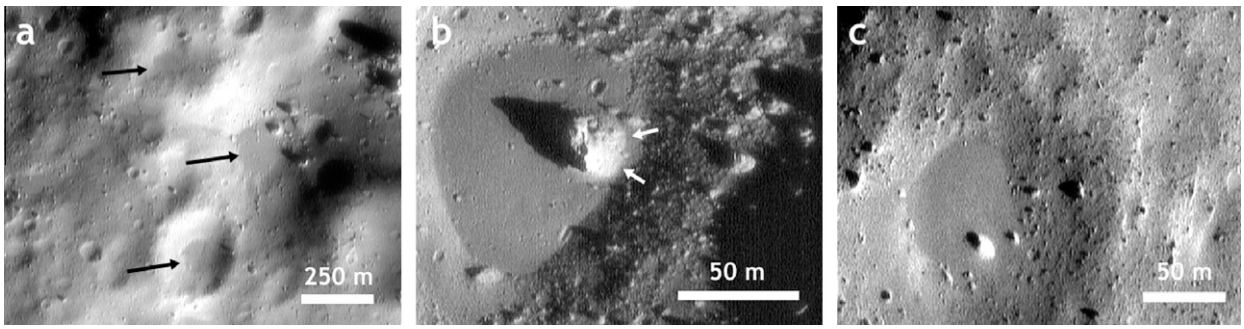

Fig. 1. Three views of ponds on Eros: (a) Multiple ponds (black arrows), the middle of which has several boulders within the bounding depression; (b) pond exhibiting characteristic flat, smooth texture, containing boulder with debris apron (white arrows); (c) pond with several associated boulders showing debris aprons. (NEAR-Shoemaker MSI images: (a) 1479,32,871, (b) 1560,87,851, (c) 1560,83,231, NASA/JHUAPL).

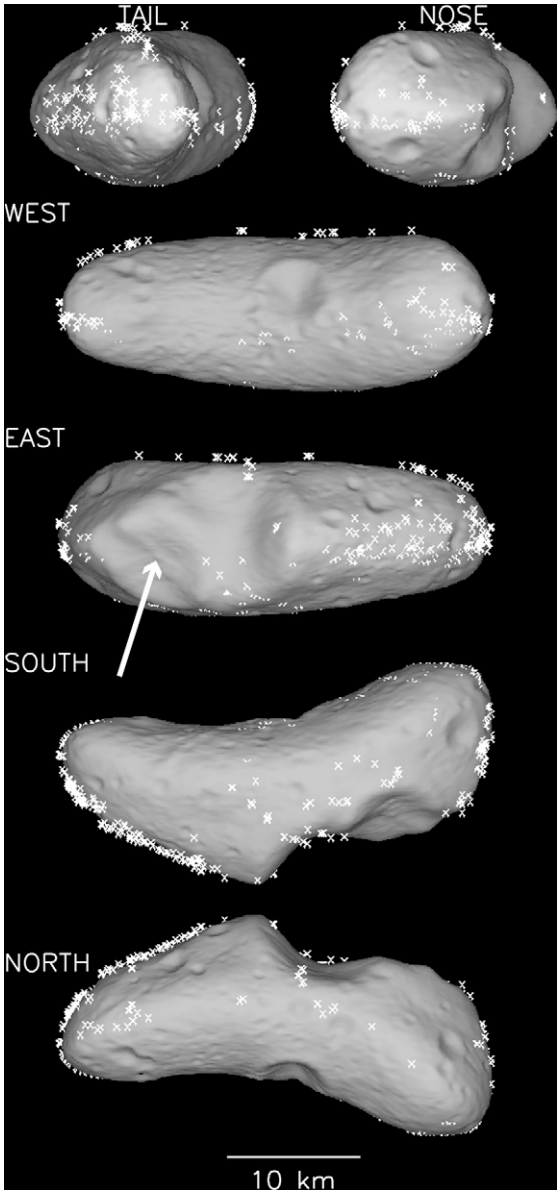

Fig. 2. Orthographic views of pond locations projected on a shaded shape model of Eros. The majority of ponds are located on the rotational equator, towards the ends of the elongated asteroid. The arrow points to Shoemaker Regio.

bottom, but this mechanism does not naturally explain the pond distribution or the color properties.

Here, we propose an alternative mechanism to supply the pond material: eroding boulders. Like other scenarios, we invoke seismic shaking to flatten and to smooth the material into a pond. In Section 2, we discuss the observations of boulders and ponds, and the relationships between them, as well as the process by which we propose boulders erode. In Section 3, we detail this new pond formation scenario. In Section 4, we cover the influence that local slope and elevation may have on the location of ponds. We finish with further discussion and propose future tests for this mechanism.

2. Observations and thermal erosion of boulders

Some boulders on Eros display what appear to be debris aprons (Fig. 1). When observed in ponds, these aprons have been interpreted as pile-up of pond material against local topography (Robinson et al., 2001). It seems doubtful, however, that the pond material could pile up against the boulders when the likely mechanism for this pile-up (seismic shaking) is also invoked to flatten and smooth material into ponds. We instead interpret the aprons as evidence that the boulders are eroding in place. Several mechanisms may produce boulder erosion, including mechanical abrasion during sliding events, micrometeorite spallation, and thermally induced disaggregation (Robinson et al., 2001). Mechanical abrasion, necessitating materials grinding past each other, is not consistent with the notion that the boulders are eroding in place; additionally, there are only a handful of examples of boulders that have rolled or slid across the surface (Prockter et al., 2002). Study of micrometeorite erosion of coherent rocks on the Moon (the best analog available) suggests that 1 m can be eroded per 1 Gyr (Crozaz et al., 1971; Arvidson et al., 1975), which is too slow to supply the required material over the age of the Solar System. Furthermore, micrometeorite bombardment may be substantially less for Eros than the Moon, because of its low gravity and its distance from any dust sources, particularly in its current Near Earth orbit. On the other hand, Pochat et al. (2009), adapting a thermal stress model from Vance et al. (2007), have explored the possibility that thermal weathering may be an important contributor to regolith formation on airless bodies. As we will now demonstrate, we therefore favor thermal erosion, unless micrometeorite erosion rates were more than 1–2 orders of magnitude greater when Eros was in the Asteroid Belt.

The process we envision is thermal fatigue. Fatigue is a well-understood materials process that results in 90% of the failures of engineered metals on Earth (e.g., Callister, 2003). (It is in fact the reason why airplane windows have rounded corners.) Fatigue is caused by a cyclical forcing of a material, which generates cumulative, microscopic damage that, after enough cycles, can seriously compromise the strength of the material, even though the stress

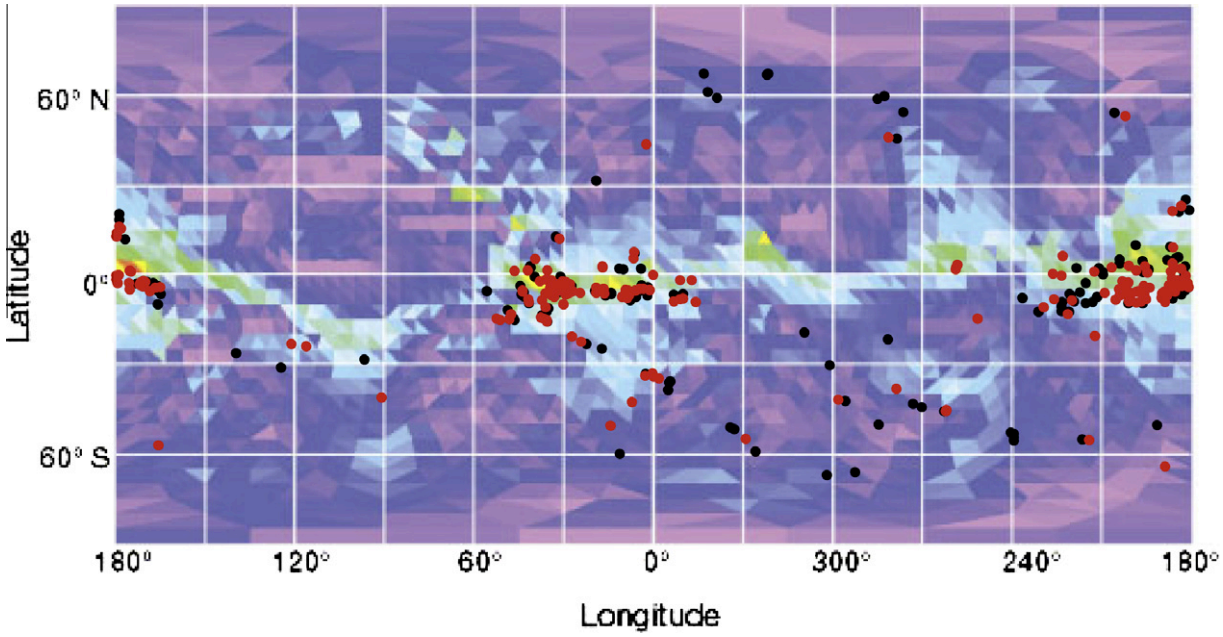

Fig. 3. A simple cylindrical projection of a plate model of Eros, where the colors represent the relative amount of time (red – more time; violet – less time) a plate is illuminated between 85° and 90° incidence angle (i.e., near the terminator, which is a necessary prerequisite for terminator passage) over the span of a year on Eros. The figure, originally from Robinson et al. (2001), is adapted to include the locations of 334 ponds in the current pond database. Ponds with associated boulders are shown with red dots, while ponds without boulders are shown with black dots.

levels are below the non-fatigued strength. On the microscopic level, cracks form and lengthen at points of high stress concentration within the structure of the material; for natural, composite materials such as are found in a boulder, material and geometric singularities that can lead to such concentrations will be ample. There are two main types of fatigue. For low-cycle fatigue, the number of cycles the material can withstand is generally less than 10^4–10^5, because the stresses are sufficient to cause widespread plastic deformation. In the high-cycle regime, the stresses can be largely absorbed elastically, thus requiring far more cycles to cause fatigue; for these materials, there is generally significant weakening by 10^8 cycles or less.

Applied to rocks, this is not a new idea. Thermal fatigue, where the source of the cyclical stresses is restricted thermal expansion/contraction, has been invoked as a potentially significant erosional source of rocks in cold, arid regions on Earth, particularly regions where the aridity precludes freeze–thaw effects (Hall, 1999), indicating that thermal cycling in a natural environment can cause silicate boulders to disaggregate. In this paper, the author also reviewed the literature, particularly the engineering literature, which goes back nearly two centuries. Notably, a major factor in driving the process is the differential thermal expansion between the mineral grains that compose a real rock, which consequently depends on the relatively subtle variations in thermal–mechanical properties of neighboring mineral grains. Thus, thermal fatigue may be even more efficient in a boulder composed of ordinary chondritic material (especially in an environment bereft of other weathering processes), because at least one thermal–mechanical property of a component of this "rock" is expected to be orders of magnitude different.

The observed geographic distribution of boulders matches the predicted ejecta distribution from the impact that formed Shoemaker Regio (Fig. 2), and thus the boulders likely represent material ejected from Eros's interior during large impacts (Thomas et al., 2001). Given that the S-type asteroids like Eros are thought to be the parent bodies of ordinary chondrites (see Foley et al., 2006 and references therein), these meteorites are then plausibly samples of boulders. Thus, we assume that the boulders are composed of silicate-rich chondrules of order 1 mm in size, held in a more metal-rich matrix (see Kuebler et al., 1999).

The relevant thermomechanical properties (e.g., yield strength, Young's modulus, coefficient of thermal expansion) of the silicates and free metals in an ordinary chondrite are surprisingly similar, except for the thermal diffusivity, which is typically two orders of magnitude greater in a metal. Thus, thermal fatigue process, which operates on Earth in rocks composed of purely silicate minerals (Hall, 1999), may be more efficient in the boulders on Eros. As a boulder on the surface crosses the terminator, the flash of sunlight would send a thermal pulse that would produce differential heating of the near-surface. The resultant differential expansion would simultaneously squeeze the chondrules and matrix, a situation that would be reversed as the boulder passes back into darkness. This process operates on the scale of the chondrules (few mm) and does not require the deep penetration of a thermal pulse (there does not need to be a connected matrix pathway into the interior). After a sufficient number of cycles and weakening, the chondrules, surrounding matrix, or both are damaged enough that this layer can slough off. A relatively thin dust/regolith cover could effectively shield an intact boulder, and thus it is likely only on fairly clean surfaces (e.g., boulder sides) where this can operate. Indeed, terminal descent images from NEAR-Shoemaker show the sides of boulders to be relatively clean (Veverka et al., 2001a). Additionally as this process is driven by the transition from light to dark (or vice versa), this naturally explains why ponds are preferentially found in areas of the asteroid that experience more terminator passages.

We can estimate the magnitude of the stresses. Study of NEAR-Shoemaker data showing temperature-dependent spectra of the sunlit surface indicates temperature variations of order 10 K (Lucey et al., 2002), while measurement of temperature of the surface of the Moon during the transition from light to dark indicated changes of order 100 K (e.g., Wieczorek and Huang, 2006). Via the Stefan–Boltzmann law, surface temperature goes as the fourth root of the absorbed solar flux. Thus given that Eros and the Moon

have similar solar distances (1.46 and 1 AU) and albedos (0.25 and 0.12), we assume that daily temperature variations on Eros are of order 10–100 K (cf. a temperature differential of order 10 K that can cause significant thermal erosion of boulders on Earth (Hall, 1999)). Thermal stress is proportional to the Young's modulus of the material and the thermal strain (coefficient of thermal expansion times the temperature difference). Assuming a Young's modulus of order 100 GPa and a thermal expansion coefficient of 10^{-5} K^{-1}, the thermal stresses will be of order 10–100 MPa, below the likely intact failure strength of the material (of order 100 MPa), which indicates these boulders are eroding in the high-cycle fatigue regime if thermal stresses are the driver.

There may be further evidence of erosion in the boulder population itself. One of us (PCT) has constructed a database of all boulders on Eros larger than 15 m, and in places down to <0.1 m in size (cf. Thomas et al., 2001). We show a size-frequency plot in Fig. 4, which plots the total number of boulders greater than a given width. Fragmentation populations like the boulders on Eros can generally be described by a cumulative size-frequency power-law ($N \propto D^{-b}$), which would plot as a straight line in log–log space (Melosh, 1989). The boulder distribution clearly cannot be fit by a single power-law. The distribution, however, may be consistent with a model where the boulders are supplied by a few boulder forming events coupled with an erosion model. We assume the boulder production function obeys a power-law.

Experiments of collisional disruption of intact and fragmented targets (Davis and Ryan, 1990; Ryan et al., 1991), perhaps the best analog to the late-stage, low-energy ejecta of large impacts that likely produces the boulder population on Eros (Thomas et al., 2001), suggests power-law exponents b from ~1 to large values of ~6 (and perhaps as large as 9!). Larger fragments of ejecta tend to possess larger values of b. As we will discuss below, the medium size (~10–80 m) and large size boulders can be well fit with two power-law curves with b values of ~3 and ~6, respectively. While it is easy to envision processes that could preferentially deplete smaller boulders after their emplacement (erosion via many mechanisms being an example), it is harder to imagine a process that preferentially depletes larger boulders, resulting in a lower initial b value (grouped boulders indicating a larger boulder fragmenting apart are rare). Thus, the initial b value was likely $\geqslant 3$, and we employ $b = 6$ to our boulder production, matching the observed large boulder population. We can model the boulders being emplaced in a single event, in multiple events, or continuously.

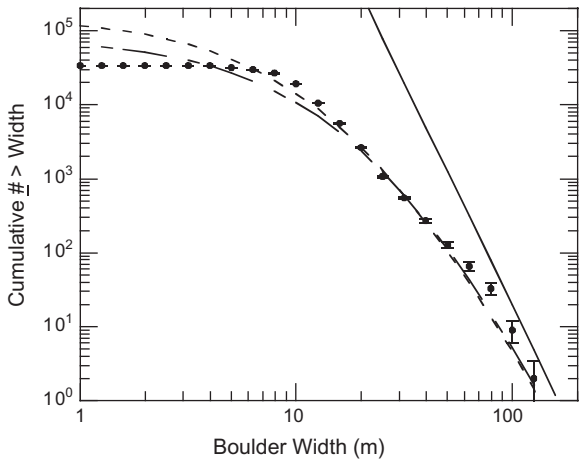

Fig. 4. A cumulative size-frequency plot of 33,939 boulders on Eros. The points are the counts; the error bars are the roots of the counts. The rollover for boulders less than ~10 m is likely an observational bias. The lines are simulation results using a boulder-emplacement/erosion model (see text). The solid line is the assumed boulder production function. The lower dashed curve shows the case where the boulders are emplaced in a single event and are subsequently eroded at a rate where 1 m of material is eroded in 8% of the time since the boulder emplacement event. The upper dashed curve shows the case where the boulders are supplied in two equal events and the erosion time scale is 5% the time since the older boulder emplacement event.

We also apply a simple erosion model. Disaggregation by thermal cycling (or micrometeorite erosion, for that matter) operates on a scale smaller than the dimensions of the boulders in the database. Thus, we assume a constant erosion rate where a meter of material is etched off a boulder in some model time, regardless of boulder size. While the erosion rate is constant, smaller boulders will disappear faster than larger ones. Disaggregating a meter of material off a 2-m boulder will result in complete erosion, while etching a meter off a 100-m boulder leaves a boulder 98% as large in terms of width and 94% in terms of volume. Removing a meter off the larger boulder, however, produces more material than off the smaller boulder (~30,000 m^3 versus ~4 m^3). For this simple model, we do not include the effects of burial or shielding by liberated material that blankets the intact boulder.

Fig. 4 also shows our model results. The solid curve is the boulder production function at the end of the simulation (i.e., the boulder population assuming no erosion). The lower dashed curve shows the case where the boulders are emplaced in a single event and are subsequently eroded at a rate where 1 m of material is eroded in 8% of the time since the boulder emplacement event. The upper dashed curve shows the case where the boulders are supplied in two equal events and the erosion time scale is 5% the time since the older boulder emplacement event. The fits are respectable, especially given the simplicity of the model. While the models do show a rollover at small sizes, due to complete erosion of small boulders, the curves diverge from the observed boulder population at the smallest sizes (less than ~10 m); however, this divergence is more likely a sampling bias introduced by the resolution of the images.

Although not shown, a model case where the boulders are emplaced continuously results in a boulder population seemingly obeying a power-law with a value of b only slightly less than that of the boulder production function (i.e., nearly coincident with the solid line in Fig. 4). This result suggests that the boulders were emplaced in a fairly small number of events, which is to be expected. Impacts large enough to produce boulders (e.g., the impact that formed Shoemaker Regio (Thomas et al., 2001)) will only happen occasionally on Eros. In addition, this simple model provides a way to estimate the erosion rate. For instance if most of the handful of large impacts formed during the billions of years Eros was in the Asteroid Belt (see Veverka et al., 2000; Cheng et al., 2001), then the time scale for sufficiently large impacts on Eros is 0.5–1 Gyr. Consequently, the time scale to erode 1 m of material is of order 10–100 Myr, significantly shorter than the micrometeorite erosion rate on the Moon (Crozaz et al., 1971; Arvidson et al., 1975). Chondrules are a few mm across, and based on the current spin state of Eros (rotating once every 5.27 h), the surface goes through of order 10^3 thermal cycles per year (it is unlikely the spin period has evolved enough to change this order of magnitude estimate). Thus, it might take of order 10^8 thermal cycles to disaggregate a layer of chondrules from a boulder on Eros, entirely consistent with a material in a high-cycle fatigue regime (Callister, 2003).

There are, of course, other interpretations of the boulder population. If we assume the characteristics of small boulders less than ~10 m is an observational bias, then the data can be well fit by two power-law curves, with $b = 3.1$ for boulders less than ~80 m, and $b = 6.1$ for larger boulders. Although larger values of b are permitted, the lower b value is more consistent with the collisional disruption experiments (Davis and Ryan, 1990; Ryan et al., 1991), and the power-law exponent for large boulders may instead indicate a depletion of large boulders likely during their implantation. Boulder erosion is not assured based on the observed boulder

population; however, the correspondence with the observation of debris aprons around boulders suggests erosion is a strong possibility. Thus if a boulder lies in a local depression, the eroded material may be trapped and serve as source material for a pond.

There is evidence that boulders and ponds are related. Large blocks on Eros (>30 m across), inferred to be ejecta from the most recent large impact that created Shoemaker, are observed to lie in an equatorial band (Thomas et al., 2001), their distribution in many ways is similar to areas that show large time spent near the terminator (Fig. 3). Furthermore, histograms of the number of ponds in bins of pond width indicate that ponds with associated boulders tend to be larger than ponds that lack boulders (Fig. 5). For these histograms, we have examined all 334 ponds in the Thomas pond database, looking for boulders (see Fig. 3 for locations of ponds with and without boulders). We define a boulder as a feature that can clearly be identified as spatially localized, with sharply rising, positive topography, which is primarily determined by image resolution. For instance, a single bright pixel with an adjoining dark pixel opposite the Sun direction, although arguably an unresolved boulder, is not so identified. Large boulders are easy to find; small boulders (less than ~10 pixels across) can be somewhat subjective. We track those cases where the identification is marginal; histograms incorporating these uncertain identifications are not qualitatively different. We employ two classifications: ponds with no obvious boulders, and ponds with boulders either within the boundaries or within one pond-radius of the boundaries. The logic here is that while a boulder may sit on the slope of the bounding depression in which the pond is found, seismic shaking will migrate the pond material to an equipotential low as it flattens the material. Additionally, fits of scaled, log-normal distributions, using the number in each bin and the bin centers, are overlaid on the histograms.

In general, ponds with associated boulders tend to be larger than ponds without boulders (median value of 66.4 m versus 40.6 m). Note that there is not a 1:1 correlation between pond size and the size of the bounding depression (cf. ponds in Fig. 1), so this difference is not simply larger bounding depressions collecting more boulders. Moreover, the number of ponds with boulders falls off less rapidly with increasing pond size (skewness of 2.4 versus 2.2). Only a limited number (16 out of 83, or ~19.3%) of ponds >75 m wide lack boulders. These differences between the two classes of ponds are consistent with the notion that boulders supply the pond material. Based on volume arguments, a smaller pond would require a smaller boulder, and a smaller boulder would erode faster. It naturally follows, then, that there would be a higher probability of observing a small pond without a boulder, because the boulder may have already eroded away.

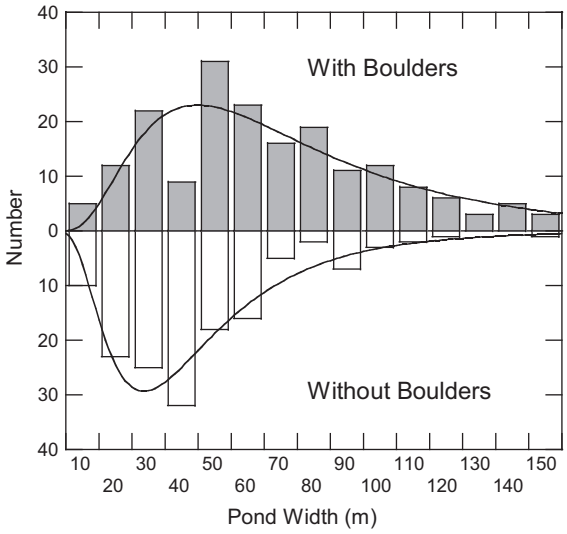

Fig. 5. Histograms of the number of ponds with widths within 10-m wide bins centered on the indicated values, from a database of 334 ponds on Eros. The total pond population is split into two cases: those ponds with associated boulders and those ponds without. Fits of log-normal distributions are also shown. There exist four ponds >155 m in width; all four have associated boulders. In general, ponds with associated boulders tend to be larger than ponds without boulders.

3. A new mechanism

Based on our observations, we propose a new scenario for the formation of ponds (Fig. 6). (1) A boulder or boulders are delivered to a local depression. (2) The boulders erode in place, creating the aprons around boulders. (The mechanism in Step 2 is not specified; we favor thermal erosion because we expect other mechanisms, such as micrometeorite erosion, to proceed too slowly.) (3) Seismic shaking flattens the material into the pond morphology, removing the apron from around the boulders and exposing them to further erosion. This scenario may be consistent with the observed bimodal distribution (Fig. 5): smaller ponds would require smaller boulders. The observation that the distribution of ponds without obvious associated boulders tend to be smaller may suggest that boulders in these ponds have already eroded sufficiently to be unobservable.

Given that boulders are likely delivered to the surface in a small number of discrete events, the ages of ponds may tend to cluster around a few discrete values. There will be some dispersion in ages, however, due to burial or blanketing slowing the erosion rate differently for different boulders and due to the fact that the strength of seismic shaking will be variable across the surface, in general being stronger nearer an impact (Cheng et al., 2002a).

Volume estimates of material in ponds can be converted into equivalent boulder sizes, which can then be compared with the observed boulder population on Eros. The vast majority of ponds do not have NEAR Laser Rangefinder (NLR) profiles that run across them, but we have identified 4 NLR profiles that run across ponds near their middles, which allow us to determine the characteristics of the bounding depression and estimate pond volume. To achieve this, we fit a parabola to the laser-shot points flanking the pond (Fig. 7), and use this parabola to calculate a volume of revolution. Cheng et al. (2002a) also determined a depth of ~6 m for a pond

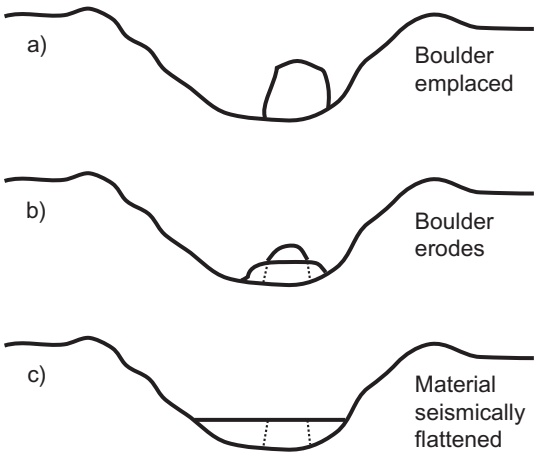

Fig. 6. Schematic representation of proposed pond formation scenario. (a) A large impact delivers a boulder into a local depression. (b) Thermal cycling disaggregates the boulder. (c) The liberated material is flattening into the pond morphology via seismic shaking. The buried (and thus preserved) remnant of the boulder is shown with dashed lines.

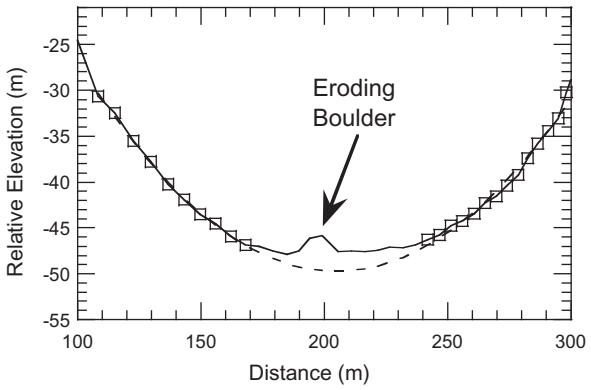

Fig. 7. NLR profile near the center of a pond ~69 m wide. The solid line is the full profile. The squares are those laser shots used to fit a parabola to the NLR profile (dashed line). This pond is thus ~2.5 m deep, with a volume of ~4670 m^3. The NLR profile also samples an eroding boulder in the center of the pond. Elevation derived from NLR shots taken between mission elapse times of ~1559,82,230 s to ~1559,82,260 s.

~90 m across, which permits a volume estimate. This volume can be converted into an equivalent boulder width. On average, the ratio of height to width of boulders is 0.55, based on 623 boulders in the Thomas boulder database that have associated height measurements. Thus, we approximate the volume of a boulder as an oblate spheroid half as tall as it is wide. Volume estimates for ponds and associated equivalent boulder volumes are shown in Table 1. The resultant boulder sizes are consistent with the observed boulder population (cf. Fig. 4). Of course, the pond material does not need to be supplied by a single boulder, but could be supplied by several smaller boulders (although as noted above, partial erosion of a large boulder can provide much more material than complete erosion of a much smaller boulder). Additionally, the boulder need not be completely eroded. The NLR profile shown in Fig. 7 samples a seemingly eroded boulder with dimensions of ~25 × 15 × 2 m, with a volume of ~393 m^3. The volume of material in this pond is estimated at ~4670 m^3; adding volumes, the observed boulder could be a remnant of a larger boulder ~59 × 35 × 5 m. Similarly, the ~90-m wide pond investigated by Cheng et al. (2002a) also possesses an apparently eroded boulder sampled by an NLR profile. Its dimensions are ~15 × 10 × 5 m, with an equivalent volume of ~393 m^3, suggesting that this boulder is the remnant of a larger boulder with dimensions ~55 × 37 × 18 m. At erosion rates of 1 m per 10–100 Myr, these remnant boulders suggest time scales of order 100 Myr to 1 Gyr, consistent with the notion that boulders are delivered to the surface in a few large impact events. Clearly, a larger boulder will take longer to erode than a smaller boulder, yet even partially eroding a large boulder can liberate a lot of material. Both of these factors may explain the observation that larger ponds tend to possess associated boulders.

A corollary of this new mechanism is that the pond material is composed of liberated chondrules and matrix, which naturally satisfies the requirement based on images that the material be sub-cm in size. (Even micrometeorite erosion, presuming it may have operated orders of magnitude faster when Eros was in the Asteroid Belt, might mechanically segregate grains [chondrules versus matrix] from the boulders.) In addition, the color characteristics of ponds would, under this scenario, result from the lack of space weathering on material recently liberated from a boulder interior, seismic sorting of the silicate-rich chondrules from the denser, more metal-rich matrix, or some combination. A mm (chondrule)-scale layer of boulder will be eroded over time scales of 10^4–10^5 years, compared with space weathering rates of within 10^6 years to reach maturity (Vernazza et al., 2009), suggesting the material is produced faster than it is space-weathered. Seismically induced flow of thermally disaggregated material from boulders not confined to a local depression will be divergent, which will disperse the unweathered material, diluting the color characteristics. Furthermore, the eroded material in a divergent flow may not permit the density stratification that leaves a lag of silicate-rich material on top.

Table 1
Pond volume estimates.

Pond width (m)	Pond volume (m^3)	Equivalent boulder width (m)
36	305	11
41	990	16
42	1040	16
69	4670	26
90	19,100	42

4. Influence of local slope and elevation

The proposed scenario is suggestive, but it does not naturally explain the pond distribution. We do note that our proposed erosion mechanism is driven by the thermal fatigue that results as a boulder transitions between sunlight and darkness. Consequently, this mechanism for delivering pond material, like the dust levitation mechanism, will be more efficient in regions that have more terminator passages (Fig. 3, cf. Robinson et al., 2001). Other factors undoubtedly play a role. It has been noted that ponds tend to be found in regions of low gravitational acceleration (Robinson et al., 2001); however, it is unclear if this association is due to lower gravity or because regions of low gravity are also regions of higher elevation. Thus to further understand the origin of ponds, we explore their relationships to local slope and elevation.

Local slope and elevation are determined on Eros using the techniques developed by Thomas (1993) and Cheng et al. (2002a,b), where the surface of Eros is referenced to an equipotential surface calculated from a shape model of the asteroid and using known spin parameters, producing true gravitational elevations and slopes. When the shape is referenced to an equipotential, the surface of Eros is, in general, relatively flat, with few areas at high or low elevation or at high slope. Thus to minimize this bias, the pond distributions are normalized by the total slope and elevation distributions over the entire asteroid; this normalization is similar to the method employed by Thomas et al. (2002) for analyzing boulder distributions found in the largest craters on Eros.

The results (Fig. 8) indicate that ponds are typically located on shallow slopes and at higher elevations. Higher elevations on Eros tend to be located out towards the bulbous ends of the asteroid. These ends of the asteroid are also regions of lower surface gravity and regions with more terminator passages (cf. Fig. 3). Thus, lower gravity or twilight conditions may control to some degree the locations of ponds (Robinson et al., 2001). Although the role that low gravity may have has not been explained, the role of lighting conditions has been suggested, by providing illumination conditions more conducive to the electrostatic transport of dust (Robinson et al., 2001; Colwell et al., 2005; Haugsjaa and Colwell, 2006; Hughes et al., 2008). Conversely, these lighting conditions provide more opportunities for thermal fatigue.

There are, however, other explanations, possibly related to the concentration of ponds at higher elevations. The presence of ponds at higher elevations may be because little loose and highly mobile regolith is present at these locations. Successive seismic shaking events should cause mobile regolith to migrate to lower elevations, leaving a thinner, less mobile regolith (i.e., that portion more resistant to seismic displacement) in higher elevation regions. This situation could lead to a contrast between the resistance to seismic

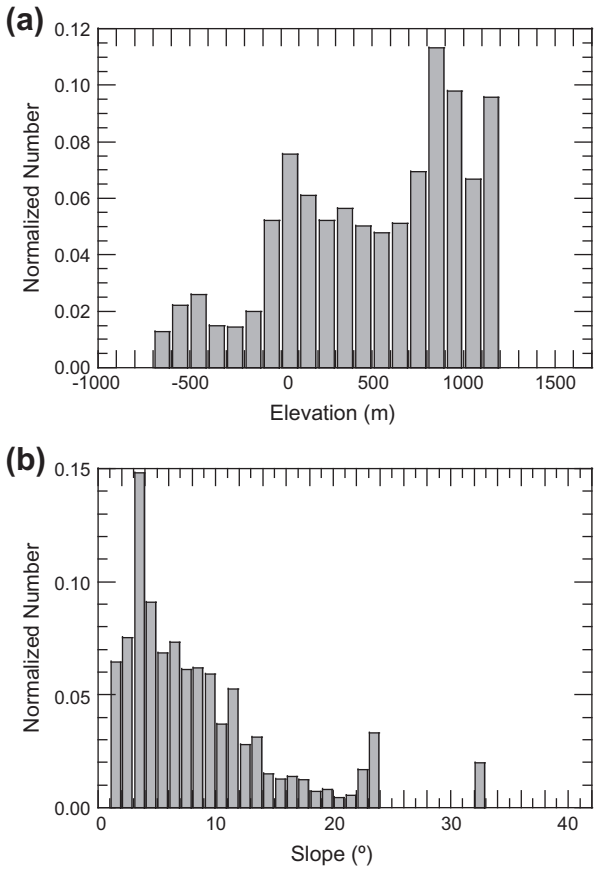

Fig. 8. Number of ponds on Eros in equal-area sized bins as a function of elevation (a) and regional slope (b), normalized by the amount of area of the surface that exists at a particular elevation or slope. Ponds tend to be located at higher elevations and lower regional slopes.

shaking of pond material and the material that makes up the bounding depression. Indeed, modeling of seismic shaking assuming uniform mechanical properties reveals that the entire depression simply becomes muted and the pond morphology does not form (Richardson et al., 2004, 2005), suggesting that a contrast in mechanical properties is required for pond formation. Conversely, the lack of ponds at low elevations may simply reflect the large amounts of mobile regolith in these regions that easily submerge the depressions in which ponds occur. Indeed, the floors of Shoemaker and Himeros possess fewer depressions than other areas of the asteroid (e.g., Thomas and Robinson, 2005).

Ponds also tend to be located in areas of low regional slopes. The low slopes ensure that source material captured in the ponds does not escape during seismic shaking. Ponds may be found on local slopes, but only when the bounding depressions represent local minima. We have identified NLR profiles of ponds that exist on sloped terrain (Fig. 9). Unlike ponds that exist in regions of low slope (or are strongly confined to the bounding depression), which tend to be gravitationally flat, ponds found on regional slopes also tend to possess a slope, with the downhill side kissing the downhill lip of the bounding depression. These observations suggest two immediate consequences. First, successive seismic shaking events will cause the uphill pond material to migrate towards the downhill side, resulting in the material emptying out of the depression. Second, it suggests that multiple seismic shaking events are needed to flatten the material into the pond morphology, because if the pond morphology could be developed in a single event, these ponds would also be flat, filling the local minima.

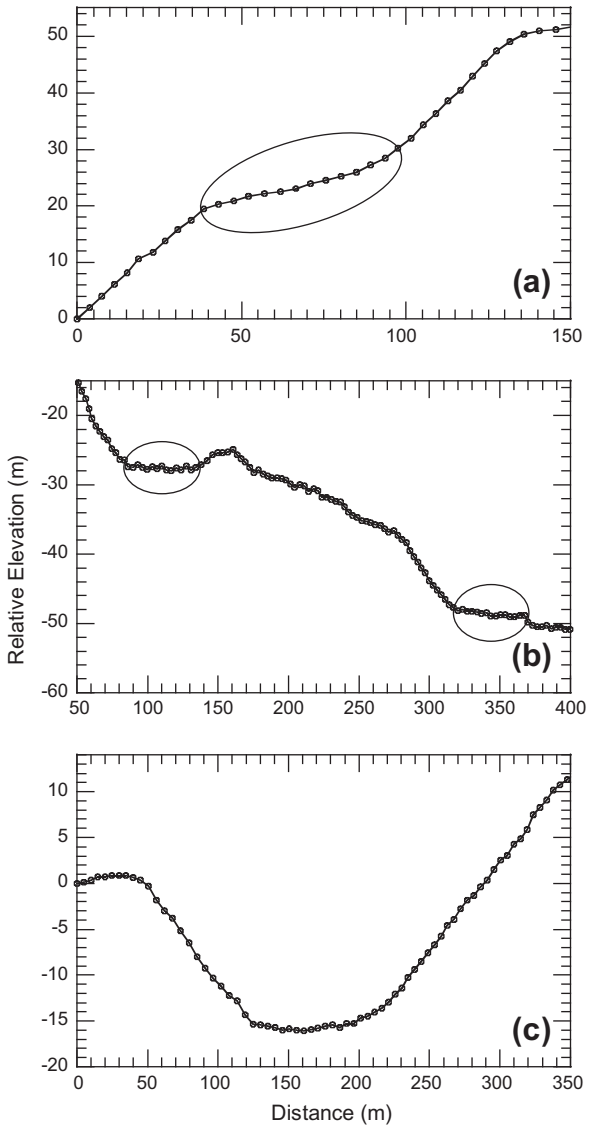

Fig. 9. NLR profiles over ponds on various regional slopes. (a) This ~40-m wide pond (highlighted by an oval), located at −3.3°N 27.5°W, rests on a regional slope of ~20°. The pond kisses the lip of the bounding depression and thus possesses its own slope of ~7°. Elevation derived from NLR shots taken between mission elapse times (METs) of ~1558,83,790–1558,83,810 s. (b) These two ponds (highlighted by ovals), located near −6°N 350°W, are both ~40 m wide and rest on a regional slope of ~6°. The pond on the left is confined to the bounding depression and so is flat (slopes <1°), while the pond on the right kisses the lip of the bounding depression and possesses a small but detectible slope of ~1.25° (METs ~ 1548,02,250–1548,02,310 s). (c) This ~75-m wide pond, located at −5.6°N 27.9°W, is strongly confined to its bounding depression on a regional slope of only ~2°, its surface varying by less than ~1 m over its width (METs ~ 1560,83,480–1560,83,510 s).

5. Discussion and future tests

We have proposed a mechanism by which there exists a causal relationship between boulders and ponds on Eros. A boulder, if caught within a bounding depression composed of material more resistant to seismic shaking and lying on locally low slopes, may supply the pond material. Like the electrostatic levitation model (Colwell et al., 2005), this model invokes seismic shaking to flatten the material to the pond morphology. Our work is motivated by our observations of boulders and ponds on Eros and not by any possible shortcomings of other models, and so we recognize the possibility of a hybrid model, where both mechanisms are important contributors. In addition, any model must contend with the

possibility of an electrostatic cohesiveness of dust-sized particles in the low gravity of Eros. A thin, cm-scale layer of dust (thinner than could have been seen in the terminal descent images from NEAR-Shoemaker) clinging to the sides of boulders could conceivably shield the boulders from thermal erosion, and this cohesion may limit the ability of dust-sized pond material delivered by levitation to be flattened seismically. (Dominance of seismic shaking over electrostatic clinging solves both of these problems.) Furthermore, any model must eventually explain the relative dearth of ponds. There are large areas on Eros that witness prolonged terminator passages and are hence conducive to dust transport, and there are >33,000 boulders. Yet, there exist only ~300 identified ponds. The disparity of these numbers suggests the process that creates ponds is relatively inefficient, any destructive mechanism is relatively efficient, or both.

The presence of ponds on Eros is observed to be unique in the Solar System, not being commonly observed on other small bodies; however, the conditions that lead to pond formation are likely not unique. According to our model, which is based on thermal disaggregation of ordinary chondritic boulders, pond formation is to be expected on the S-type asteroids. This prediction seemingly rules out "ponds" on comets and terrestrial bodies like Mercury or the Moon, but this presupposes that the structure of the chondrites makes them more susceptible to thermal fatigue than the rocks found on the Moon or Mercury (as stated above, thermal cycling is a potentially significant erosional source of "normal" silicate rocks in cold, arid regions on Earth (Hall, 1999)). Even if these rocks are as susceptible to thermal fatigue, however, the erosion rate would likely be slower than micrometeorite erosion, because the length of day on the Moon and Mercury is two orders of magnitude longer than a day on Eros. Conceivably, the thermal erosion mechanism could operate on all types of chondrites, assuming there is a strong enough contrast in thermomechanical properties between the chondrules and the matrix. Thus, ponds are a possibility on Mathilde (C-type) and the satellites of Mars (spectral affinity to D-type), assuming they are indeed captured asteroids. In contrast, the low metal content of carbonaceous chondrites might make boulders on darker asteroids more resistant to thermal fatigue. Regardless, the highest-resolution images of Mathilde by the NEAR-Shoemaker spacecraft (160 m/pixel) were insufficient to observe ponds (Veverka et al., 1999). Phobos and Deimos, on the other hand, have been imaged with resolutions of a few meters. We have only found ambiguous, at best, examples on Phobos. If ponds are truly absent on the satellites of Mars, their lack may be due to the differing compositional and environmental conditions between these satellites and the S-type Eros, including the thermal environments. Because of its anticipated icy surface, similar ponded deposits are likely absent from Ceres, a target of NASA's Dawn mission (Russell et al., 2006). Dawn may observe ponds on Vesta's lunar-like surface, but only if ponds on Vesta are significantly larger than on Eros (expected image resolution of Dawn at Vesta is ~70 m/pixel). Left with the S-type asteroids, the potential exists for observations of ponds on Annefrank, Dactyl, Gaspra, Ida, and Itokawa. Of these, only Itokawa has been observed at sufficiently high resolution to reveal ponds (Cheng et al., 2007). Pond-like features have been observed (smooth deposits that appear flat relative to an equipotential surface). The highest resolution images, however, indicate a cobbly surface, lacking particles larger than cm-scale (Cheng et al., 2007), so the material that makes up these pond-like features is likely not delivered via dust transport or boulder erosion. Furthermore, these scale materials may not be expected on Itokawa. A simple calculation comparing the solar radiation pressure on a dust particle on Itokawa and the gravitational weight of the particle suggests radiation pressure may be sufficient to clean the surface of the asteroid of dust (particles of order 100 μm or smaller). In addition, the dearth of craters suggests a very youthful age for the surface, possibly young enough that only limited thermal erosion may have occurred. Moreover, small particles may have drained into Itokawa's porous interior.

There are future tests that can be performed. To distinguish between the boulder erosion and dust transport mechanisms, the simplest and by far most expensive experiment would be to fly a new mission to Eros capable of mm-scale imagery and spectroscopy, in order to determine whether the pond material is mm-sized (i.e., chondrules) or finer (i.e., dust). Other tests are currently possible for lower cost. Seismic shaking experiments (e.g., Izenberg and Barnouin-Jha, 2006) may reveal the conditions under which the pond morphology can be created and possibly destroyed, and may elucidate the mechanical properties of the materials that form both the ponds and their bounding depressions. Clearly, tests of the proposed thermal erosion mechanism via material fatigue are also required. Thermomechanical models are hampered by the fact that the thermal and mechanical properties of meteorites are poorly known, and what is known for the bulk meteorite does not distinguish between chondrules and matrix (e.g., Flynn, 2004). Moreover while the properties of the constituents of these meteorites are known, the complex structure likely limits the utility of models to coarse estimates. Thus, the most fruitful avenue would be thermal cycling (fatigue) experiments on ordinary chondrites. We further note that this erosion process is a previously unrecognized mechanism for generating regolith on S-type asteroids.

Acknowledgments

We thank A.F. Cheng for discussions that helped shape this paper, and C.R. Chapman and an anonymous reviewer for comments that improved our arguments. This work was supported in part by NASA DDAP Grant #NNG05GG94G to LMP and NASA DDAP Grant #NNG06GF58G to OSB.

References

Arvidson, R., Crozaz, G., Drozd, R.J., Hohenberg, C.M., Morgan, C.J., 1975. Cosmic ray exposure ages of the features and events at the Apollo landing sites. Moon 13, 67–69.

Callister Jr., W.D., 2003. Materials Science and Engineering: An Introduction, sixth ed. John Wiley and Sons, New York. 820pp.

Cheng, A.F., and 11 colleagues, 2001. Laser altimetry of small-scale features on 433 Eros from NEAR-Shoemaker. Science 292, 488–491.

Cheng, A.F., Izenberg, N., Chapman, C.R., Zuber, M.T., 2002a. Ponded deposits on Asteroid 433 Eros. Meteorit. Planet. Sci. 37, 1095–1105.

Cheng, A.F., Barnouin-Jha, O., Prockter, L., Zuber, M.T., Neumann, G., Smith, D.E., Garvin, J., Robinson, M., Veverka, J., Thomas, P., 2002b. Small-scale topography of 433 Eros from laser altimetry and imaging. Icarus 155, 51–74.

Cheng, A.F., Barnouin-Jha, O.S., Hirata, N., Miyamoto, H., Nakamura, R., Yano, H., 2007. Fundamentally distinct outcomes of asteroid collisional evolution: Itokawa and Eros. Geophys. Res. Lett. 34, L09201. doi:10.1029/2007GL029559.

Colwell, J.E., Gulbis, A.A.S., Horányi, M., Robertson, S., 2005. Dust transport in photoelectron layers and the formation of dust ponds on Eros. Icarus 175, 159–169.

Crozaz, G., Walker, R., Woolum, D., 1971. Nuclear track studies of dynamic surface processes on the Moon and constancy of solar activity. Proc. Lunar Sci. Conf. 2, 2543–2558.

Davis, D.R., Ryan, E.V., 1990. On collisional disruption: Experimental results and scaling laws. Icarus 83, 156–182.

Flynn, G.J., 2004. Physical properties of meteorites and interplanetary dust particles: Clues to the properties of the meteors and their parent bodies. Earth Moon Planets 95, 361–374.

Foley, C.N., Nittler, L.R., McCoy, T.J., Lim, L.F., Brown, M.R.M., Starr, R.D., Trombka, J.I., 2006. Minor element evidence that Asteroid 433 Eros is a space-weathered ordinary chondrite parent body. Icarus 184, 338–343.

Hall, K., 1999. The role of thermal stress fatigue in the breakdown of rock in cold regions. Geomorphology 31, 47–63.

Haugsjaa, A.L., Colwell, J.E., 2006. Modelling electrostatic dust transport on Eros. Lunar Planet. Sci. 37. Abstract 1225.

Hughes, A.L.H., Colwell, J.E., DeWolfe, A.W., 2008. Electrostatic dust transport on Eros: 3-D simulations of pond formation. Icarus 195, 630–648.

Izenberg, N.R., Barnouin-Jha, O.S., 2006. Laboratory simulation of surface seismic effects on low gravity bodies. Lunar Planet. Sci. 37. Abstract 2017.

Kuebler, K.E., McSween Jr., H.Y., Carlson, W.D., Hirsch, D., 1999. Sizes and masses of chondrules and metal–troilite grains in ordinary chondrites: Possible implications for nebular sorting. Icarus 141, 96–106.

Lucey, P.G., Hinrichs, J., Kelly, M., Wellnitz, D., Izenberg, N., Murchie, S., Robinson, M., Clark, B.E., Bell III, J.F., 2002. Detection of temperature-dependent spectral variation on the Asteroid Eros and new evidence for the presence of an olivine-rich silicate assemblage. Icarus 155, 181–188.

Melosh, H.J., 1989. Impact Cratering: A Geologic Process. Oxford Univ. Press, New York. 245pp.

Pochat, N.G., Vance, S., Collins, G.C., 2009. Thermal weathering on airless planetary surfaces. Am. Geophys. Union, Fall Mtg. Abstract P23C-1289.

Prockter, L., Thomas, P., Robinson, M., Joseph, J., Milne, A., Bussey, B., Veverka, J., Cheng, A., 2002. Surface expressions of structural features on Eros. Icarus 155, 75–93.

Richardson, J.E., Melosh, H.J., Greenberg, R., 2004. Impact-induced seismic activity on Asteroid 433 Eros: A surface modification process. Science 306, 1526–1529.

Richardson Jr., J.E., Melosh, H.J., Greenberg, R.J., O'Brien, D.P., 2005. The global effects of impact-induced seismic activity on fractured asteroid surface morphology. Icarus 179, 325–349.

Riner, M.A., Eckart, J.M., Digilio, J.G., Robinson, M.S., 2006. Global study of small-scale color features on 433 Eros, the effect of residual scattered light and implications for ponded deposit formation mechanisms. Lunar Planet. Sci. 37. Abstract 2291.

Robinson, M.S., Thomas, P.C., Veverka, J., Murchie, S., Carcich, B., 2001. The nature of ponded deposits on Eros. Nature 413, 396–400.

Robinson, M.S., Thomas, P.C., Veverka, J., Murchie, S.L., Wilcox, B.B., 2002. The geology of 433 Eros. Meteorit. Planet. Sci. 37, 1651–1684.

Russell, C.T., and 20 colleagues, 2006. Dawn Discovery mission to Vesta and Ceres: Present status. Adv. Space Res. 38, 2043–2048.

Ryan, E.V., Hartmann, W.K., Davis, D.R., 1991. Impact experiments. 3: Catastrophic fragmentation of aggregate targets and relation to asteroids. Icarus 94, 283–298.

Thomas, P.C., 1993. Gravity, tides, and topography on small satellites and asteroids: Application to surface features of the martian satellites. Icarus 105, 326–344.

Thomas, P.C., Robinson, M.S., 2005. Seismic resurfacing by a single impact on the Asteroid 433 Eros. Nature 436, 366–369.

Thomas, P.C., Veverka, J., Robinson, M.S., Murchie, S., 2001. Shoemaker crater as the source of most ejecta blocks on the Asteroid 433 Eros. Nature 413, 394–396.

Thomas, P.C., and 18 colleagues, 2002. Eros: Shape, topography, and slope processes. Icarus 155, 18–37.

Vance, S., Harnmeijer, J., Kimura, J., Hussmann, H., Demartin, B., Brown, J.M., 2007. Hydrothermal systems in small ocean planets. Astrobiology 7, 987–1005.

Vernazza, P., Binzel, R.P., Rossi, A., Fulchignoni, M., Birlan, M., 2009. Solar wind as the origin of rapid reddening of asteroid surfaces. Nature 458, 993–995.

Veverka, J., and 13 colleagues, 1999. NEAR encounter with Asteroid 253 Mathilde: Overview. Icarus 140, 3–16.

Veverka, J., and 32 colleagues, 2000. NEAR at Eros: Imaging and spectral results. Science 289, 2088–2097.

Veverka, J., and 38 colleagues, 2001a. The landing of the NEAR-Shoemaker spacecraft on Asteroid 433 Eros. Nature 413, 390–393.

Veverka, J., and 32 colleagues, 2001b. Imaging of small-scale features on 433 Eros from NEAR: Evidence for a complex regolith. Science 292, 484–488.

Wieczorek, M.A., Huang, S., 2006. A reanalysis of Apollo 15 and 17 surface and subsurface temperature series. Lunar Planet. Sci. 37. Abstract 1682.